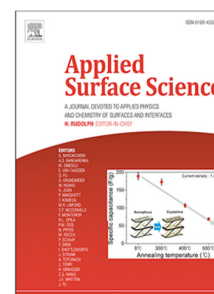


Journal Pre-proof

Scanning-resonance optical sensing based on a laterally graded plasmonic layer – optical properties of $\text{Ag}_x\text{Al}_{1-x}$ in the range of $x = 0$ to 1

Benjamin Kalas, György Sáfrán, Miklós Serényi, Miklós Fried, Péter Petrik



PII: S0169-4332(22)02298-X
DOI: <https://doi.org/10.1016/j.apsusc.2022.154770>
Reference: APSUSC 154770

To appear in: *Applied Surface Science*

Received date : 23 April 2022
Revised date : 16 August 2022
Accepted date : 31 August 2022

Please cite this article as: B. Kalas, G. Sáfrán, M. Serényi et al., Scanning-resonance optical sensing based on a laterally graded plasmonic layer – optical properties of $\text{Ag}_x\text{Al}_{1-x}$ in the range of $x = 0$ to 1, *Applied Surface Science* (2022), doi: <https://doi.org/10.1016/j.apsusc.2022.154770>.

This is a PDF file of an article that has undergone enhancements after acceptance, such as the addition of a cover page and metadata, and formatting for readability, but it is not yet the definitive version of record. This version will undergo additional copyediting, typesetting and review before it is published in its final form, but we are providing this version to give early visibility of the article. Please note that, during the production process, errors may be discovered which could affect the content, and all legal disclaimers that apply to the journal pertain.

© 2022 The Author(s). Published by Elsevier B.V. This is an open access article under the CC BY license (<http://creativecommons.org/licenses/by/4.0/>).

1
2
3
4
5
6
7
8
9
10
11
12
13
14
15
16
17
18
19
20
21
22
23
24
25
26
27
28
29
30
31
32
33
34
35
36
37
38
39
40
41
42
43
44
45
46
47
48
49
50
51
52
53
54
55
56
57
58
59
60
61
62
63
64
65

Scanning-resonance optical sensing based on a laterally graded plasmonic layer – optical properties of $\text{Ag}_x\text{Al}_{1-x}$ in the range of $x = 0$ to 1

Benjamin Kalas^{a,b}, György Sáfrán^a, Miklós Serényi^a, Miklós Fried^{a,c}, Péter Petrik^{a,d}

^a*Institute for Technical Physics and Materials Science, Centre for Energy Research, Konkoly-Thege Rd. 29-33, 1121 Budapest, Hungary*

^b*Doctoral School of Physics, Faculty of Science, University of Pécs, 7624 Pécs, Ifjúság útja 6, Pécs, Hungary*

^c*Institute of Microelectronics and Technology, Óbuda University, Tavaszmezo u. 17, 1084 Budapest, Hungary*

^d*Department of Electrical and Electronic Engineering, Institute of Physics, Faculty of Science and Technology, University of Debrecen, 4032 Debrecen, Hungary*

Abstract

Plasmonic $\text{AgAl}/\text{Si}_3\text{N}_4$ sensor layer structure was deposited on a fused silica glass slide by dual DC magnetron sputtering. The composition of the $\text{Ag}_x\text{Al}_{1-x}$ layer was laterally graded in which x linearly changes from $x = 0$ to $x = 1$ over a distance of 20 mm. The Si_3N_4 layer serves both as a resonator and a protective layer providing homogeneous chemical properties on top of the inhomogeneous AgAl layer. The structure was illuminated through a hemi-cylinder for variable-angle measurements in the Kretschmann-Raether configuration using a focused spot that enabled the change of x by moving it along the gradient of the composition. Optical properties of $\text{Ag}_x\text{Al}_{1-x}$ in the whole composition range were obtained. The positions of resonant peaks were shifted by changing the angle and the lateral position of the spot in a flow-cell configuration. The optical sensing performance of the bilayer system was investigated for $x=0$ and $x=1$. Based on the capabilities of ellipsometry limit of detection in refractive index unit values of $\approx 4 - 8 \cdot 10^{-6}$ can be achieved in the resonant positions utilizing both p- and s-polarizations. Due to the flexible tunability of the resonant wavelengths by moving a focused spot, the above sensitivity is available in-situ, over the spectral range of 265-1504 nm.

1
2
3
4
5
6
7
8
9 *Keywords:* Combinatorial material science, spectroscopic ellipsometry,
10 plasmonics, biosensing
11
12

13 **1. Introduction**

14
15 Plasmonics is the field of research and technology that introduces the inter-
16 actions between the electric field component of incident light and free electrons
17 in metallic thin films or various metallic nanostructures [1]. At the interface
18 of metal layers and dielectrics (e.g. air or liquids), plasmons interacting with
19 light result in a surface plasmon polariton (SPP) resonance: originating from a
20 strongly confined surface wave that propagates along the interface and decays
21 exponentially in both the metal film and the dielectric ambient.
22
23

24
25 An effective method for tuning the optical response of metallic thin films
26 and nanostructures, i.e., to subtly customize the optimum wavelength range for
27 SPP, the chemical composition of the plasmonic material is modified by alloying
28 various metals [2, 3, 4, 5, 6]. Originally, for SPP applications noble metals such
29 as Ag, Au and Pt have been the preferred choice owing to their abundant free
30 electrons despite the well-known optical losses introduced by interband optical
31 transitions [7, 8, 9]. In the past few years, however, earth-abundant metals, such
32 as Al and Mg, have also been used as a new class of materials for low-optical-loss
33 and low-cost optical components [10]. For on-chip nanophotonics applications,
34 metals like Al and Cu are ideal choices since their fully complementary metal-
35 oxide-semiconductor (CMOS) compatibility along with their abundance on earth
36 result in low-cost device processing [6]. Furthermore, pertaining to the large
37 free electron densities observed in metal alloys and intermetallics, they are also
38 promising choices as alternative plasmonic materials [7].
39
40

41
42 Alloying of metals via physical deposition methods lead to almost arbitrary
43 tunability regarding their optical behavior in the ultraviolet-visible-near infrared
44 (UV-Vis-NIR) wavelength range. This flexible control of the spectrum has also
45 enabled the further development of a variety of advanced optoelectronic devices,
46 such as switches [11] and biosensors [12]. It has been shown earlier that alloying
47
48
49
50
51
52
53
54
55
56
57
58
59
60
61
62
63
64
65

1
2
3
4
5
6
7
8
9 Ag or Au with another metal that contributes two or three electrons per atom
10 to the free electron gas can significantly modify the reflection and absorption
11 spectra [13].
12
13

14 As an example the investigation of single-phase Ag-Cu with different compo-
15 sition has led to the conclusion that the optical properties of these alloys could
16 be efficiently manipulated by the annealing temperature and the composition
17 thus making Ag-Cu an attractive material for plasmonics [14]. The dielectric
18 properties of a number of alloy systems, such as Au-Ag [3, 15], Ag-Cu [3, 14]
19 and Au-Cu [3] have been examined using optical spectroscopy, and a combinato-
20 rial gold-aluminium ($\text{Au}_x\text{Al}_{1-x}$) layer has also been introduced previously [16].
21 Several examples for alloys with possible use in the field of plasmonics have also
22 been presented in Ref. [17].
23
24
25
26
27

28 Ag is routinely used in various applications due to its excellent optical and
29 electrical characteristics. Ag has the most favorable properties for plasmonic
30 applications of any material in the VIS-NIR range [17], and is widely available.
31 However, the thickness and surface roughness of an Ag layer can significantly
32 influence these advantageous properties [18], inducing unfavorable deviations
33 compared to an ideal Ag layer. The island formation during thin Ag film growth
34 [19] ultimately lead to a rough and semicontinuous layer with additional optical
35 loss due to excitation of plasmon resonances [20]. It is known that Ag follows the
36 Volmer-Weber growth model [21] in which the deposited Ag atoms initially form
37 isolated islands. As the deposition continues, these islands grow further and
38 eventually connect to form a semicontinuous layer. To overcome this problem, a
39 1–2 nm thin germanium (Ge) layer can be deposited under the Ag layer [22, 23].
40 This method has led to a reduced surface roughness value and a decreased
41 percolation threshold for Ag nanofilms (the latter being 10-20 nm typically
42 without the additional Ge layer [24]). However, Ge has high absorption in the
43 visible wavelength range which subsequently leads to a reduced transmittance.
44 To address this situation the deposition of an ultra thin and smooth Ag film
45 has been reported previously [25], which shows both low optical loss and low
46 electrical resistance. This film has been made by involving the co-deposition of
47
48
49
50
51
52
53
54
55
56
57
58
59
60
61
62
63
64
65

1
2
3
4
5
6
7
8
9 only a small amount of Al during Ag deposition without any wetting layer. In
10 the same study it has been found that the incorporation of a small amount of
11 Al suppressed the 3D island growth of Ag and resulted in the formation of an
12 ultra thin layer with a reduced surface roughness of 1 nm and also a reduced
13 percolation threshold of 6 nm. As a promising application, ion-implanted Al-Ag
14 bimetallic substrate has been proposed as an excellent tool for surface enhanced
15 fluorescence (SEF) measurement [26].
16
17
18
19

20 Al layer with a high reflectivity throughout the Vis spectral range has been
21 used in optical reflector applications [27]. An Al-Ag alloy-film is also a highly
22 reflective coating which can be used for solar reflectors [28]. The effect of Al
23 on the optical properties of Ag has also been investigated in a 500-nm layer
24 deposited on silicon surface [29]. In the same work a slight blue-shift of the bulk
25 plasma frequency has been observed with increasing Al ratio. It has also been
26 shown that a 7-nm Al-doped Ag film remains stable under ambient conditions
27 for over six months without any protective layer [30]. Al-doped Ag offers ad-
28 ditional benefits when compared to pure Ag, such as ultrathin film formation,
29 enhanced thermal and long-term stability, better adhesion with substrates, and
30 improved 3D nanostructure coverage [31, 30]. In addition, its optical loss can
31 be further reduced by a simple annealing treatment. It has also been shown
32 that the central position of the interband transition around 1.5 eV is tunable
33 with variable annealing temperatures and different Ag concentrations in Al-Ag
34 alloys [32, 33]. All these merits facilitate the fabrication of high-performance Al
35 plasmonic structures [34, 35] along with long range surface plasmon polariton
36 (LR-SPP) waveguides [30].
37
38
39
40
41
42
43
44
45
46

47 In this paper, we introduce a thin and smooth combinatorial $\text{Ag}_x\text{Al}_{1-x}$ alloy
48 film with x including the whole composition range $0 \leq x \leq 1$ deposited by dual
49 DC magnetron sputtering using a scaled-up device [36]. The optical properties
50 of the deposited $\text{Ag}_x\text{Al}_{1-x}$ alloy film were characterized by variable angle spec-
51 troscopic ellipsometry (VASE) in a wide wavelength (λ) range. The intermetal-
52 lic layer was realized on a fused silica (FS) substrate and it was subsequently
53 covered with a radio-frequency (RF) sputtered Si_3N_4 layer. This additional
54
55
56
57
58
59
60
61
62
63
64
65

1
2
3
4
5
6
7
8
9
10
11
12
13
14
15
16
17
18
19
20
21
22
23
24
25
26
27
28
29
30
31
32
33
34
35
36
37
38
39
40
41
42
43
44
45
46
47
48
49
50
51
52
53
54
55
56
57
58
59
60
61
62
63
64
65

90 layer serves dual purposes acting as a protecting layer preventing the interaction between the metal layer/air interface and as a waveguide layer to realize a coupled plasmon-waveguide resonator (CPWR) structure [37, 38, 39, 40] in the Kretschmann-Raether (KR) configuration [41]. In this study, the emerging resonance peaks were investigated both theoretically and experimentally. Based on the calculations it was predicted that it is possible to precisely measure the refractive index change of liquids from ultraviolet wavelengths (ca. 260 nm) up to the near infrared range (ca. 1500 nm) by using a single compositionally graded sample.

It was also shown that on a single sample not only the composition of the intermetallic layer but also its thickness can be controlled in the range of 15 nm (Al-side) to 40 nm (Ag-side) for realizing a tunable plasmonic sensor structure. By moving the spot and changing the angle of incidence we realized a "scanning resonance" tool in which the wavelength position of sensitivity maxima can be scanned and adjusted during the in-situ measurement, resulting in a quantitative "high-sensitivity" spectroscopy method.

To our knowledge this is the first time that both the lateral thickness and the composition change was manipulated in a controlled way in a combinatorial thin film. It is also the first time that such a structure is used in a sensor structure the properties of which can be varied by laterally moving a focused spot over the interface in a KR configuration. More specifically, we show that not only the composition of the intermetallic layer but also its thickness can be controlled in the range of 15 nm (Al-side) to 40 nm (Ag-side) for realizing a tunable plasmonic sensor structure. By moving the spot and changing the angle of incidence this is the first time that a "scanning resonance" tool is realized in which the wavelength position of sensitivity maxima can be scanned and adjusted during the in-situ measurement, resulting in a quantitative "high-sensitivity" spectroscopy method. Our result can also be considered as a proof of concept, based on which a family of sophisticated plasmonic sensors can be built with modulation capabilities

120 2. Materials and Methods

2.1. Deposition of the combinatorial sensor structure

Combinatorial $\text{Ag}_x\text{Al}_{1-x}$ alloy film was deposited on a 25 mm \times 10 mm (width \times length) and 150 ± 25 μm thin UV-grade FS substrate (purchased from Valley Design Corp) by "single-sample" micro-combinatory at room temperature. The deposition resulted in a layer with gradient composition of $\text{Ag}_x\text{Al}_{1-x}$ with x ranging in $0 \leq x \leq 1$. The 25 mm long substrate exhibits a 20 mm long gradient $\text{Ag}_x\text{Al}_{1-x}$ track enclosed between 2.5 mm long lead-in sections of one target's flux.

A stainless steel UHV system by dual DC magnetron sputtering was used which is a scaled-up device [36] originally developed for synthesizing micro-combinatorial transmission electron microscopy samples. The present arrangement sweeps a shutter with a 1 mm \times 10 mm slot in fine steps above the substrate meanwhile the power of the two magnetron sources is regulated in sync with the slot movement (Fig. 1). As the slot passes over the substrate, the fluence of Ag gradually decreases from 100% to 0%, while that of Al increases from 0% to 100%, which creates the required gradient of the composition. The maximum values of the applied power for the Ag and Al targets were 150 W and 330 W, respectively. The variable thickness was also achieved by the fine regulation of the slot movement. The capability of "single-sample" micro-combinatory has been demonstrated for amorphous $\text{Si}_x\text{Ge}_{1-x}$ thin layers recently [42, 43]. In these works, excellent composition linearity has been found along the sample position.

The main advantages of the combinatorial deposition technique are the following: (i) The deposited layer is prepared in one process step which assures that all the parameters of the sample preparation and also the substrate properties are the same - except for the modulated parameter (the composition and/or thickness). (ii) The optical measurement and the evaluation are also easier and more efficient, since they can automatically be performed by a lateral scan over the sample surface. The evaluation process also supports a single-process in-

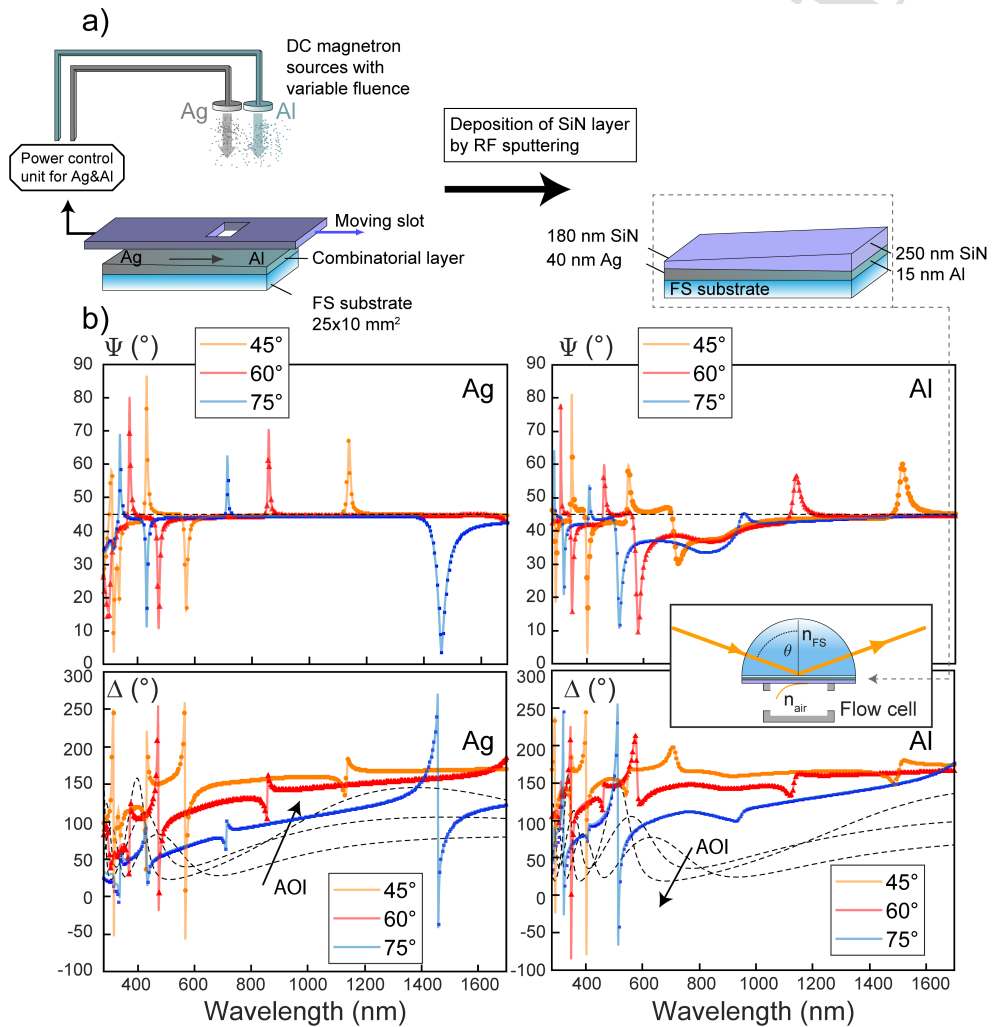


Figure 1: a) Deposition of the combinatorial Ag_xAl_{1-x} layer and Si_3N_4 layer on the top of it. b) Simulated spectra with $x = 0, 1$ (pure Al and Ag, respectively) at different angles of incidence in the KR-configuration (inset figure). Solid lines show TMM simulated results, while discrete points show FEM calculations. Black dashed curves depict the spectra for a structure without the combinatorial AgAl layer (i.e., only Si_3N_4 layer is present with thickness values of 180 nm and 250 nm, respectively).

1
2
3
4
5
6
7
8
9 150 terpretation. (iii) The combinatorial technique also allows the characterization
10 of larger modulations and unexpected variations of the properties without any
11 assumption of the lateral dependence.
12

13 The deposition of the Si_3N_4 cover layer was realized by RF sputtering, the
14 variable thickness (from 180 nm to 250 nm) of this layer was achieved by the
15 careful regulation of the linear movement of a cover-plate over the sample. To
16 155
17 minimize the disadvantageous effect of air on the metallic combinatorial layer,
18 RF sputtering was applied immediately after the $\text{Ag}_x\text{Al}_{1-x}$ alloy film deposition.
19
20
21

22 2.2. Simulated optical spectra

23
24 In order to achieve the best sensitivity in the KR-configuration, optical sim-
25 160
26 ulations were carried out to optimize the thicknesses of both the $\text{Ag}_x\text{Al}_{1-x}$ (at
27 $x = 0, 1$) alloy film and the Si_3N_4 film prior to the layer deposition. These
28 simulations were implemented using the transfer matrix (TMM) and finite el-
29 element (FEM) methods. The TMM calculations were conducted via the com-
30 mercial software CompleteEASE, and the FEM calculations were carried out
31 165
32 using COMSOL Multiphysics. For both implementations, the optical spectra
33 were calculated in the λ -range of 250 nm-1690 nm and angles of incidence (θ)
34 of 45° - 75° . The dielectric functions $\varepsilon = \varepsilon_1 - i\varepsilon_2$ [$= N^2 = (n - ik)^2$] of Ag and
35 Al are imported from Ref. [44].
36
37
38
39

40 The optimized thicknesses were carefully chosen to fulfill all the advantages
41 170
42 of the layer system: (i) realization of multiple resonance peaks in the wavelength
43 spectra at a single angle of incidence (AOI), (ii) emergence of resonance peaks
44 of both p- and s-polarization and also (iii) the possible realization of narrower
45 resonance peaks (compared to a single metallic layer) is also possible. (iv)
46 The solely changing parameter along the sample is the chemical composition
47 175
48 of the $\text{Ag}_x\text{Al}_{1-x}$ layer. The properties of the Si_3N_4 -liquid interface remain the
49 same, thus the adsorption of biological molecules would not be influenced by
50 the different composition. Si_3N_4 is a widely used material due to its excellent
51 thermal and chemical stability with a large bandgap of ≈ 5 eV [45, 46], also
52 being used for biosensor applications [47].
53
54
55
56
57
58
59
60
61
62
63
64
65

1
2
3
4
5
6
7
8
9
10
11
12
13
14
15
16
17
180 The optimal thickness value of the Ag layer was fixed at 40 nm (the reported
optimal thickness for Au in most research papers [48]), whereas in the case of
Al it was fixed at 15 nm due to its higher absorption [49]. The variation in the
thickness of the Si₃N₄ layer ($d_{SiN} = 250$ nm and 180 nm for $x = 0$ and 1 ,
respectively) was chosen in order to shift the spectral positions of the resonance
185 peaks, thus realizing sensitive regions in the widest spectral domain possible.

18 The simulated $\Psi = \tan^{-1}(|r_p|/|r_s|)$ spectra for $x = 0, 1$ in the KR-configuration
are presented in the bottom part of Fig. 1. Here Ψ denotes one of the ellip-
sometric angles, while r_p and r_s are the amplitude reflection coefficients for p-
and s-polarizations, respectively. It is notable that narrow resonance peaks with
24 both polarizations emerge for both $x = 0$ (pure Al) and 1 (pure Ag) and their
190 spectral positions vary from UV (in case of Al) to the NIR range. It is impor-
tant to emphasize that SPPs cannot be enhanced below ≈ 300 nm in case of
Ag due to its interband transitions. However, for Al the interband transition
is a spectrally localized band around 800 nm and surface plasmon resonances
195 can be realized at wavelengths higher or shorter than this value [50, 49]. The
dashed black lines in Fig. 1 show the TMM-simulated spectra for the scenario
when the combinatorial Ag_xAl_{1-x} is not present ($d_{Ag_xAl_{1-x}} = 0$), emphasizing
the profound effect of the metallic layer.

39 Further simulation calculations and results are also included in the Support-
40 ing information of present study.
200

42 43 44 45 46 47 48 49 50 51 52 53 54 55 56 57 58 59 60 61 62 63 64 65

2.3. Spectroscopic Ellipsometry

51 Spectroscopic ellipsometry (SE) is an attractive tool for thin film character-
52 ization [51]. This method is based on the measurement of both the amplitude-
53 and phase changes of the light, which is detected after its reflection on the sur-
54 face of a sample. From a measurement the ellipsometric angles, Ψ and Δ are
205 usually presented being defined by $\rho = \tan \Psi \exp(i\Delta) = r_p/r_s$, where ρ is the
complex reflectance ratio [52]. The angles Ψ and Δ are related to the amplitude
ratio and the phase difference between p- and s-polarized light, respectively.

The 25 mm \times 10 mm sample was placed in a home-built KR-cell which

1
2
3
4
5
6
7
8
9
10
11
12
13
14
15
16
17
18
19
20
21
22
23
24
25
26
27
28
29
30
31
32
33
34
35
36
37
38
39
40
41
42
43
44
45
46
47
48
49
50
51
52
53
54
55
56
57
58
59
60
61
62
63
64
65

210 consists of a FS hemicylinder. Using SE and KR-configuration together is a popular method with applications mainly in studies of real-time biological processes [53, 54]. Previously it was demonstrated that by using the same setup with a dielectric Bloch-multilayer structure, the ultraviolet wavelength range is also accessible in the reflected spectra [55]. The sample was scanned by a Woolam M-2000DI rotating compensator spectroscopic ellipsometer with a focused spot that was moved along the center line, parallel to the long edge of the sample. The measurements were carried out using a lateral resolution of 1 mm. The plane of incidence was parallel to the short edge, and the AOI was varied between 45° and 75° . The corresponding size of the focused spot was 0.3 mm wide and 0.6 – 0.9 mm long. The measurement time was a few seconds for one point and one AOI in the whole wavelength range of 250 nm -1690 nm. As a result of the applied technique we obtained, within reasonable time, high-resolution and high-accuracy maps of optical properties as a function of composition and wavelength. The spectral resolution bandwidth is around 5 nm and 10 nm in the UV/Vis and in the near infrared wavelength ranges, respectively. The spectral density of the experimental data points is about 1.6 nm and 3.4 nm in the UV/Vis and in the near infrared wavelength ranges, respectively.

The optical properties and thicknesses of the combinatoral metal layer was calculated from the measured spectra detected by SE in the KR-configuration. This method is of superior sensitivity [56] when compared to a simple measurement as illustrated with the calculated differential spectra in Fig. 2. Here the difference spectra of Ψ are presented for a 1-nm-change in the Al (15 nm \rightarrow 16 nm) and Ag (35 nm \rightarrow 36 nm) layers. It is notable that the spectral changes are significantly larger for the KR-configuration, thus measuring the optical properties in the KR-setup is definitely advantageous.

An optical model of multiple layers was constructed for an appropriate sample analysis. First, the optical properties of the Si_3N_4 layer were calculated by using the $n(\lambda) = A + B/\lambda^2 + C/\lambda^4$ Cauchy-dispersion approach. Here λ corresponds to the incident wave in vacuum in unit of μm , the parameter A is dimensionless, while B and C are in the units of μm^2 and μm^4 , respectively.

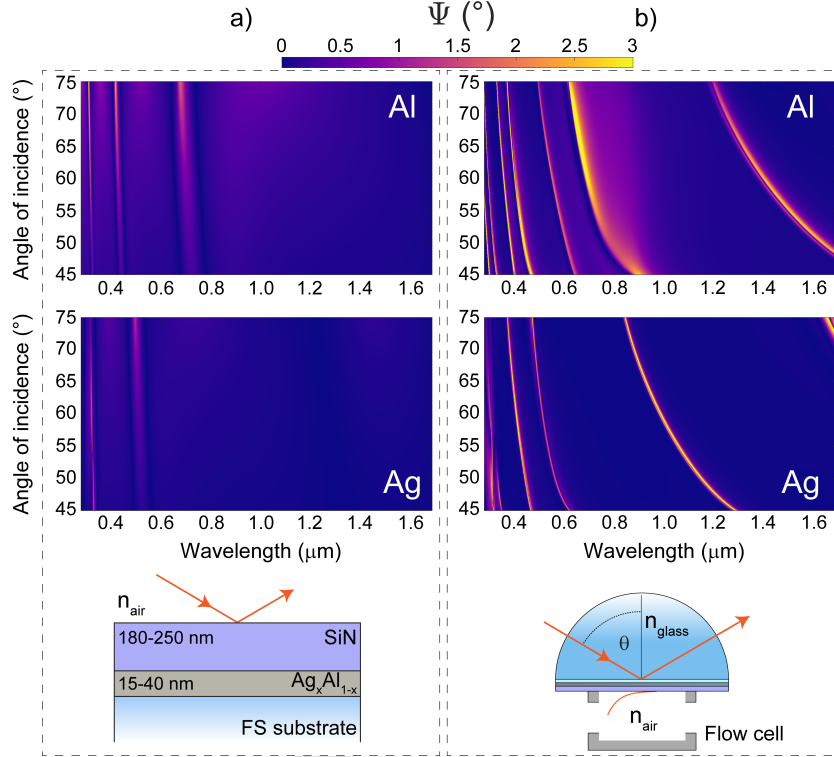


Figure 2: The simulated effect of a 1-nm thickness change in the $\text{Ag}_x\text{Al}_{1-x}$ layer at $x = 0$ using reflection configurations measuring from a) the ambient and b) from the substrate (KR-configuration).

For this investigation a 100-nm-thin Si_3N_4 layer was deposited on a Si substrate and was measured by SE. The calculated parameter values ($A = 1.903$, $B = 0.007$ and $C = 0.0005$) were then fixed during further data analysis. The optical properties of the $\text{Ag}_x\text{Al}_{1-x}$ layer were described by the Drude-Lorentz (DL) oscillator model [57, 58]. The formalism for the Drude term in the DL model was given by Ref. [59]

$$\varepsilon(E) = \varepsilon_{\text{Drude}}(E) + \varepsilon_{\text{Lorentz}}(E) = \frac{-\hbar^2}{\varepsilon_0 \rho (\tau E^2 + i\hbar E)} + \frac{A_{Lj} B_{Lj} E_{Lj}}{E_{Lj}^2 - E^2 - iEB_{Lj}},$$

where ρ [$\Omega \cdot \text{cm}$], τ [s], \hbar [eV · s] and ε_0 [$\text{F} \cdot \text{cm}^{-1}$] are the resistivity, the mean scattering time, the reduced Planck's constant and the permittivity of the free

space, respectively. In the second term A_L, B_L and E_L are the dimensionless amplitude, the broadening and the central energy (both in eV) of the Lorentzian oscillator. Here j denotes the j th oscillator. During the fit process it was found that for the Ag-rich layers an approach using Gauss-oscillators gave better results [60]. The shape of $\varepsilon_{Gauss}(E)$ was then defined as

$$\varepsilon_{Gauss}(E) = A_{Gj} \cdot \left[\Gamma_{Gj} \left(\frac{E - E_{Gj}}{\sigma_{Gj}} \right) + \Gamma_{Gj} \left(\frac{E + E_{Gj}}{\sigma_{Gj}} \right) + i \left(\exp \left\{ - \left(\frac{E - E_{Gj}}{\sigma_{Gj}} \right)^2 \right\} - \exp \left\{ - \left(\frac{E + E_{Gj}}{\sigma_{Gj}} \right)^2 \right\} \right) \right],$$

where E is the photon energy of incident light in eV, $\sigma_G = Br_G / 2\sqrt{\ln 2}$. Here, A_G is the amplitude, E_G is the center energy in eV and Br_G is the broadening in eV. Γ_G is a convergence series that produces a line shape for ε_1 in a Kramers-Kronig consistent manner [61].

During the data evaluation the sensitive oscillator parameters and thicknesses of the top two layers were fitted. The fitted values were calculated by minimizing the root mean square error (RMSE) defined by Ref. [62]

$$\text{RMSE} = \sqrt{\frac{1}{2M - P - 1} \sum_{j=1}^M \left[\left(\frac{\Delta_j^{meas} - \Delta_j^{calc}}{\sigma_{\Delta_j}^{meas}} \right)^2 + \left(\frac{\Psi_j^{meas} - \Psi_j^{calc}}{\sigma_{\Psi_j}^{meas}} \right)^2 \right]}, \quad (1)$$

where M is the number of wavelengths, P denotes the number of unknown parameters, while the subscripts 'meas' and 'calc' indicate the measured and calculated values. Here σ is the standard deviation of the measured values. A global fit on random grid with Levenberg-Marquardt algorithm [63] was used for obtaining the global minimum during the fitting process.

The RMSE values were carefully investigated and compared for both the Lorentzian- and Gaussian-approaches and it was found that starting from the Al side ($x = 0$) to $x \approx 0.4$ the Drude-Lorentz model produces better results.

2.4. Transmission electron microscopy

The microstructure of the sensor was investigated by transmission electron microscopy (TEM), high resolution TEM (HRTEM), scanning TEM (STEM),

1
2
3
4
5
6
7
8
9 high angle annular dark field (HAADF) and energy dispersive X-ray spectrometry (EDS) modes by means of a FEI Titan Themis 200 kV spherical aberration (Cs) corrected TEM with 0.09 nm HRTEM and 0.16 nm STEM resolution. The composition of the samples was measured by STEM-EDS and elemental maps
10
11
12
13
14
15
16
17 were obtained by spectrum imaging with 4 Thermo-Fischer "Super X G1" EDS detectors built in the microscope column.

18 19 20 **3. Results and discussion**

21 22 *3.1. Properties of the Ag_xAl_{1-x} layer characterized by SE and TEM*

23
24 TEM measurements were carried out on FIB cross section lamellae prepared
25
26 at four selected positions along the combinatorial sample, representing different
27
28 x compositions and thicknesses of the Ag_xAl_{1-x} and Si_3N_4 layers. Fig. 3
29 represents the TEM results achieved at a position of 9.5 mm along the sample
30
31 ($x \approx 0.65$).

32
33 TEM and SEM HAADF micrographs of the cross-section of the sample taken
34
35 at the above position shown in Figs. 3a and 3b revealed a thickness of 32 nm
36
37 and 225 nm for the Ag_xAl_{1-x} and Si_3N_4 layers, respectively. EDS measurement
38
39 of the Ag_xAl_{1-x} layer at the same position showed a composition of Ag/Al =
40
41 65/35 in terms of atomic percent. The elemental map and an EDS line-scan
42
43 across the layer system including silica/ Ag_xAl_{1-x} / Si_3N_4 /C+Pt(C) is shown in
44
45 Figs. 3c and 3d. In the line-scan, HAADF appearing in black shows the Z-
46
47 contrast change across the layers.

48
49 The thicknesses of the combinatorial metal layer and the Si_3N_4 films were
50
51 characterized by SE measurements in the KR-configuration and by TEM mea-
52
53 surements. The result of this analysis is shown in Fig. 4a. It is very conclusive
54
55 that the measured thickness values from the SE and TEM investigations are in
56
57 excellent agreement, while they are also close to the planned values along the
58
59 samples. Besides the thickness values the compositions of Al and Ag were also
60
61 obtained by TEM. The results presented in Fig. 4b indicate that the planned
62
63 linearity of composition dependence was successfully achieved.
64
65

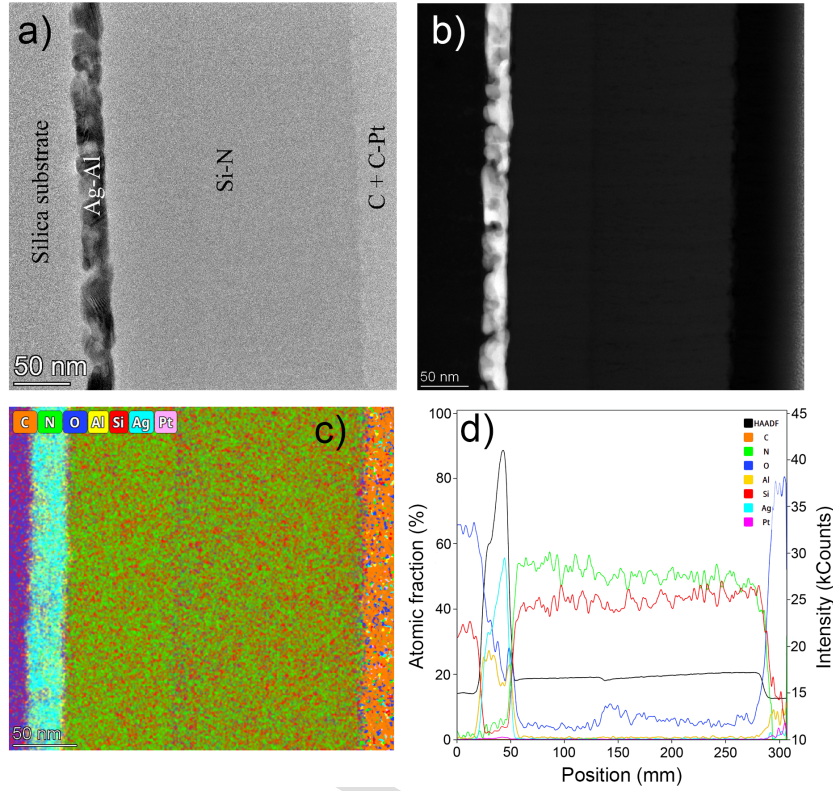


Figure 3: Cross section TEM of the sample at the position of Ag/Al=65/35 at%. (a,b) TEM and SEM HAADF image, respectively, (c) Colored EDS elemental map of the cross section of the sample, (d) A line-scan of the compositional changes (at%) across the layer system: Silica/Ag_xAl_{1-x}/Si₃N₄/C+PtC.

3.2. Composition dependence of the optical properties of the Ag_xAl_{1-x} layer

SE investigation of the Ag_xAl_{1-x}/Si₃N₄ structure was carried out parallel to the long edge of the sample with a lateral resolution of 1 mm in the KR-cell filled with air. The measured Ψ -spectra at $\theta = 47^\circ$ is presented in Fig. 5a across the λ range of 250–1690 nm. From this investigation, significant spectral changes are obtained regarding the positions and the FWHM values of the resonances indicating the huge effect of the variable metal composition. Detailed Ψ spectra were also captured for $\theta = 45$ – 55° and presented at $x \approx 0$ and 1 in Fig. 5b. The

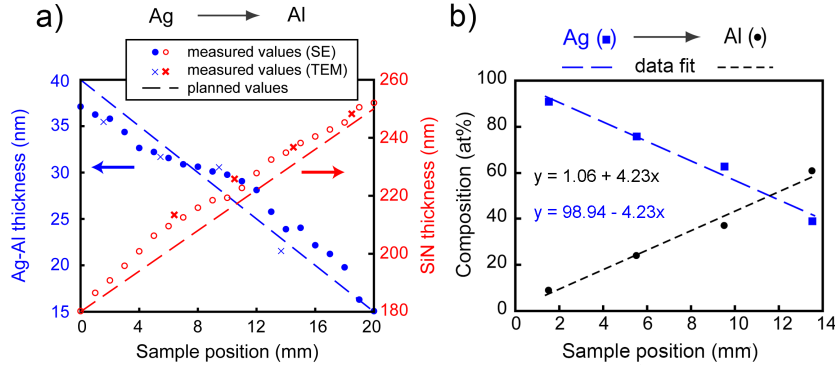


Figure 4: a) Measured $\text{Ag}_x\text{Al}_{1-x}$ and Si_3N_4 thicknesses along the sample from TEM and SE experiments. The dashed lines denote the desired trends. b) Measured position-dependence of the $\text{Ag}_x\text{Al}_{1-x}$ composition by TEM-FIB investigations.

AOI step in these figures is 0.2° .

The significance of shifting the spectral position of the resonance peaks by simply changing the position of the light spot along the sample can be advantageous for optical sensing arrangements where the angle of incidence cannot be changed. In the case of pure Ag it is also true that regardless the incidence angle, resonance peak positions have a lower limit regarding the accessible smallest wavelength value which can be further reduced only by modulating its optical properties. Also, the change of angle usually deteriorates the broadening to a larger extent than the change of composition. Finally, there are wavelength ranges that are not accessible by changing the angle of incidence.

The composition dependent dielectric functions were calculated from the fitted (Ψ, Δ) spectra that were measured in the KR-cell (Typical spectra are shown in Fig. 5c). In this analysis the oscillator parameter values and the thicknesses of the $\text{Ag}_x\text{Al}_{1-x}/\text{Si}_3\text{N}_4$ layers were fitted. The obtained complex dielectric functions are presented in Fig. 6. In Figs. 6a and 6b optical functions from $x \approx 1$ to $x \approx 0.4$ are depicted. It is to be noted that ε_2 increases when x decreases. This can be explained by the increasing amount of the Al impurities (greater electron scattering due to compositional disorder in the system) [29, 64].

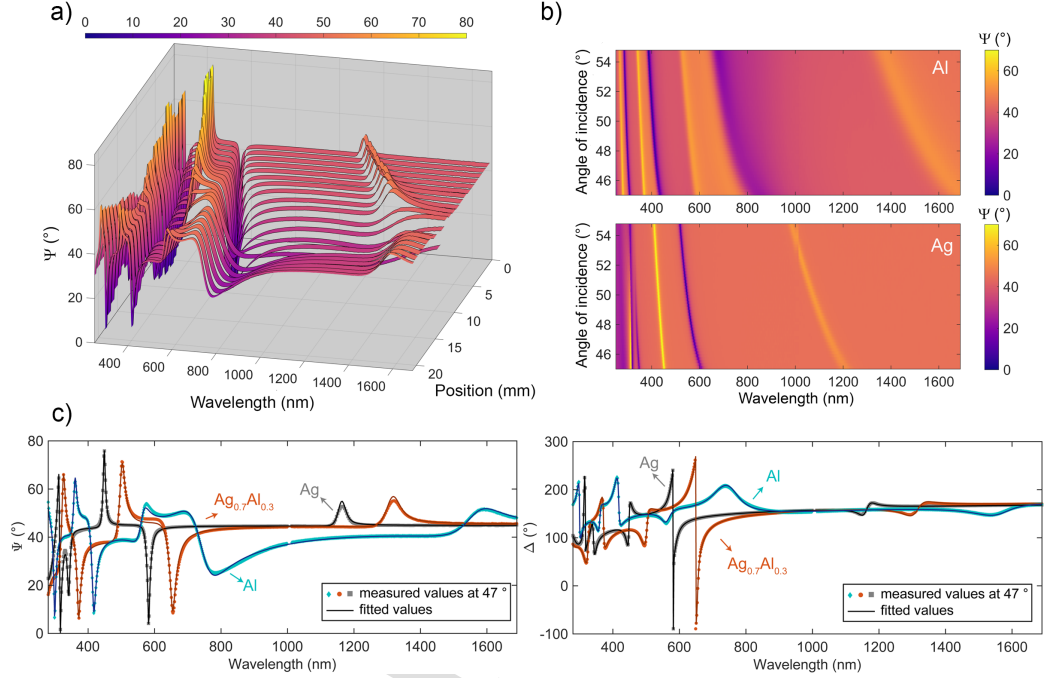


Figure 5: a) Measured Ψ -spectra along the combinatorial sample in the wavelength range of 250 – 1690 nm and at $\theta = 47^\circ$. b) Measured Ψ -spectra at $x \approx 0$ and 1 (Al and Ag in the top and bottom figures, respectively), at $\theta = 45^\circ$ - 55° . c) Typical measured Ψ and Δ spectra at $\theta = 47^\circ$ with fitted curves.

The blue-shift of the interband transitions by decreasing x is also a well-known effect [64] as well as the appearance of a new ε_2 -peak near 500 nm. This latter phenomenon can be attributed to new interband transitions [65].

Starting from the Al-rich side ($x \approx 0$), a significant change in ε_2 can be observed once again. Here, the ε_2 -peak shifts toward the smaller wavelengths as well and it can be noticed that in the NIR wavelength range the value of ε_2 decreases by the increasing value of x . In fact, the interband transition peak shifts from 740 nm ($x \approx 0$) to 485 nm ($x \approx 0.35$).

For the elucidation of these results it is vital to emphasize that not only the composition x but also the thickness of the combinatorial layer changes,

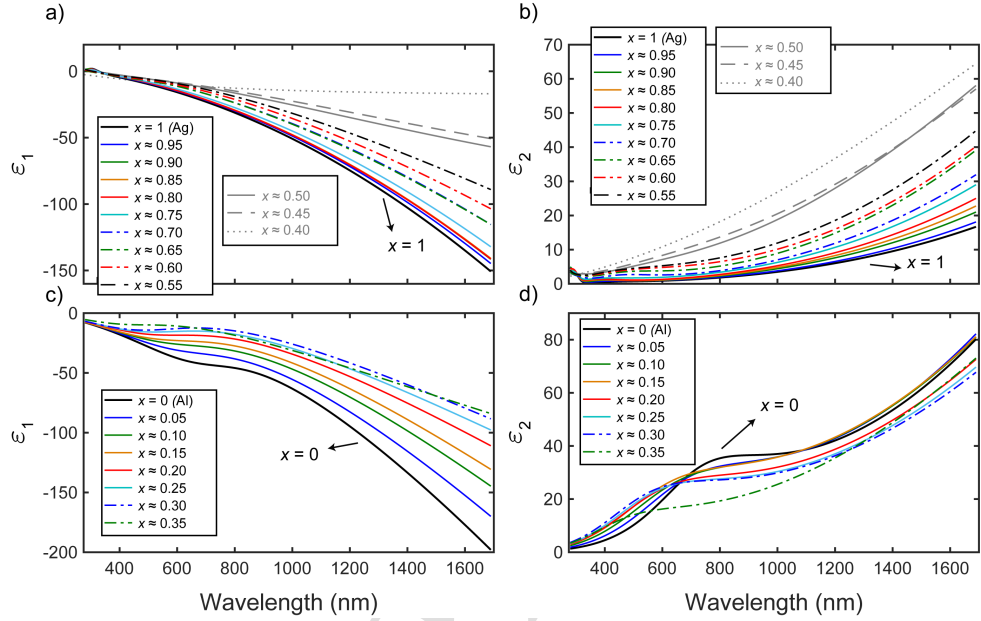


Figure 6: a) and c) ϵ_1 , b) and d) ϵ_2 values from SE measurements in the KR cell.

which bears a huge effect on the optical properties [66, 67, 68]. Besides the crystallites/grain shape and size of metal films, it is well-known that thickness can also significantly influence the optical properties when it is smaller than approximately 50 nm [69]. This effect can be attributed to the fact that the typical value of the average path of free electrons in Ag ($l = 4.375 \cdot 10^{-8}$ m [70]) is then comparable to the typical size of the crystallites. Consequently the grains size affects the average free path of the electrons and for this reason the values of and the so called free electron effect will be observable [71].

Meanwhile, it has also been shown previously that the circumstances of Al layer deposition via various techniques also have a profound influence on the dielectric function of the film since it can influence the typical grain size within a wide range (ca. 10-50 nm) [72, 73, 74].

According to the measured Ψ -spectra and the results from the optical analysis, layers with compositions $x \approx 0.40$, 0.45 and 0.50 have the most different

1
2
3
4
5
6
7
8
9
10
11
12
13
14
15
16
17
18
19
20
21
22
23
24
25
26
27
28
29
30
31
32
33
34
35
36
37
38
39
40
41
42
43
44
45
46
47
48
49
50
51
52
53
54
55
56
57
58
59
60
61
62
63
64
65

330 features among the measured points. In this x -range dielectric functions were described either by a single Drude-oscillator ($x \approx 0.4$) or with a Drude-Gauss approach ($x \approx 0.45, 0.50$). This phenomenon in the mentioned x composition range may be attributed to the phase changes described in Ref. [75].

For planar SPR applications a quality factor can be defined as $Q_{SPP} = \varepsilon_1^2/\varepsilon_2$ [76] (SPP stands for surface plasmon polariton). Calculation of Q_{SPP} can be useful for identifying the most sensitive x composition for a given wavelength range. From Ref. [17] it is evident that among various candidates Ag has the highest Q_{SPP} value ranging up to $\lambda = 10 \mu\text{m}$. However, for UV applications Al is the best choice, Q_{SPP}^{Al} being between 10 and 100 in this wavelength range. This value is highly dependent on the layer thickness of the metal layer due to its effect on the optical losses. However, it is apparent from Fig. 7c that the value $Q_{SPP}^{\text{Al}} \approx 100$ can be achieved. For Ag the Q_{SPP} value is approximately three times higher in the IR range with respect to Al (Fig. 7a). It can be noticed that the highest Q_{SPP} values were achieved for $x \approx 1$. However, for $x \approx 0.95$ the decrease in Q_{SPP} can be still tolerated.

In Figs. 7b and 7d the x composition dependence of the $\text{Im}\{-1/\varepsilon\} = \varepsilon_2/(\varepsilon_1^2 + \varepsilon_2^2)$ energy loss function is depicted that can be used for indicating the existence of electronic collective oscillators. The maximum of the $\text{Im}\{-1/\varepsilon\}$ value indicates plasma resonances in the materials [65] near to the interband transitions at 325 nm in Ag ($x = 1$). By decreasing x the value of the maximum decreases and its spectral position is blue-shifted. These trends in the results are similar to the ones that have been found for Ag-Al [77, 64] and for Ag-Cu alloys earlier [14]. Starting from $x = 0$ (Al) $\text{Im}\{-1/\varepsilon\}$ is increasing with x , which is an opposite effect than in previous results [32]. However, in the same study it was found that by increasing the layer thickness, $\text{Im}\{-1/\varepsilon\}$ also increases, which in this case seems to be the dominant effect.

3.3. $\text{Ag}_x\text{Al}_{1-x}$ layer for optical sensor applications

The fabricated sensor structure has optimized thicknesses only at compositions $x = 0$ (pure Al) and $x = 1$ (pure Ag), because the optical properties of

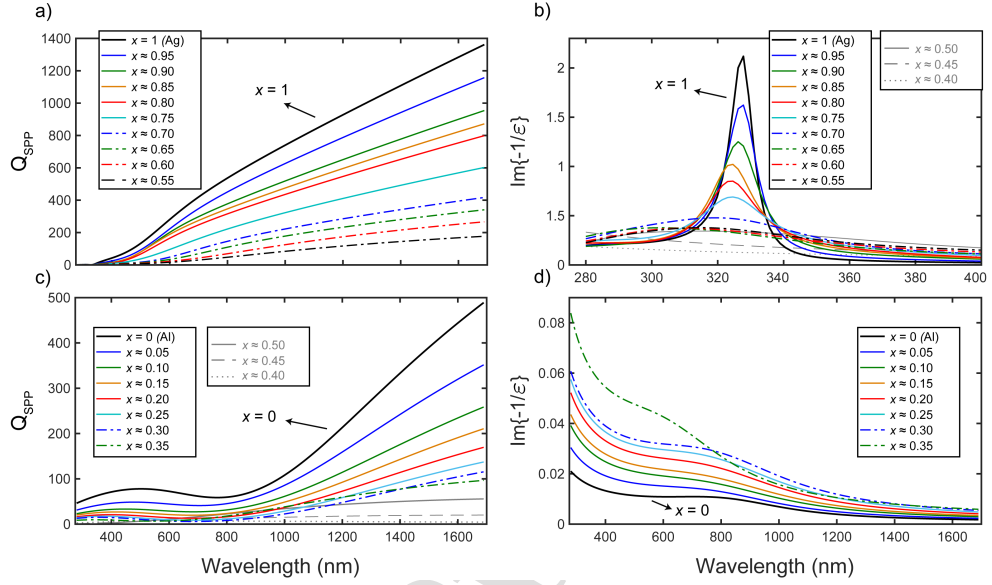


Figure 7: a) and c) Calculated Q_{SPP} , b) and d) calculated $\text{Im}\{-1/\epsilon\}$ values from SE measurements. Note that the layer thickness is not constant for the different compositions.

360 these pure phases were considered to be more reliable than the references for
 361 mixed phases. After the determination of the optical properties for all the x
 362 values, it would be possible to optimize the lateral thickness profile, but our
 363 one-sample combinatorial device is currently only optimized for linearly graded
 364 compositions and thicknesses. The utilization of both arbitrary composition
 365 and thickness profiles can be a next step in the development process, published
 366 in a following paper.

To demonstrate the sensitivities of the ellipsometric angles at both $x = 0$ and
 370 $x = 1$, results from TMM-calculations are presented in Fig. 8. The spectral
 differences in both Ψ and Δ were calculated in the wavelength range of 250–
 1700 nm and the AOI range of 40–75°. The shift in the spectra stemmed from
 a $\Delta n_{air} = 10^{-3}$ refractive index change in the ambient air. Sensitive regions
 emerge for both layer structures making them ideal candidates for gas-sensing
 applications. (The differences in the spectra presented in Figs. 1 and 8 are

1
2
3
4
5
6
7
8
9
10
11
12
13
14
15
16
17
18
19
20
21
22
23
24
25
26
27
28
29
30
31
32
33
34
35
36
37
38
39
40
41
42
43
44
45
46
47
48
49
50
51
52
53
54
55
56
57
58
59
60
61
62
63
64
65

due to the different n_{FS} values being used in the simulations. For Fig. 1
375 $n_{FS} = 1.5$ without any dispersion, while for Fig. 8 n_{FS} was described by using
the Sellmeier term imported from Ref. [55]. The origin of the resonance peaks
are the same as described earlier, however, their spectral positions are slightly
shifted.)

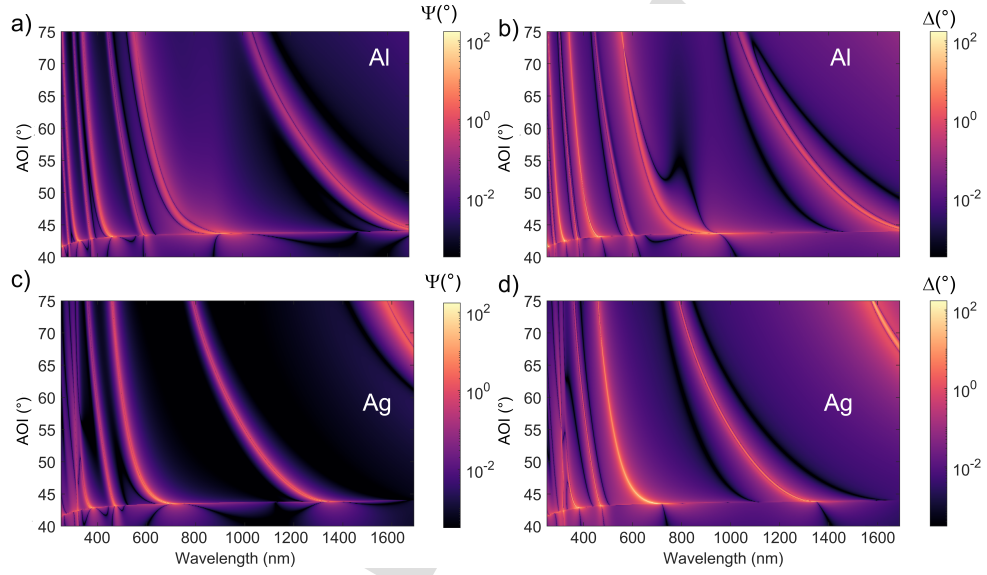


Figure 8: TMM-calculated differences in (Ψ, Δ) spectra for a $\Delta n_{air} = 10^{-3}$ change. Sub-figures a) and b) stand for Al, while sub-figures c) and d) for Ag.

The same calculations were also computed in an aqueous ambient for $\theta = 65$ –
380 75° (Fig. 9). Here, the refractive index of water (n_{water}) was chosen to be
1.312 and its change was $\Delta n_{water} = 10^{-4}$. A theoretical limit of detection
(LOD) value was estimated (by using a typical noise value σ_{meas} from a real
measurement) from these results as the smallest detectable bulk refractive index
change using the expression $LOD = 3 \cdot \sigma_{meas} / S$. Here, S denotes the sensitivity
52
53
54
55
56
57
58
59
60
61
62
63
64
65

385 defined as $S = \Delta\Delta / \Delta n_{water}$. (Since the sensitivity of Δ is usually higher
than that of Ψ , thus in this analysis all values were calculated using the phase
information.) The calculated LOD values for the Al and Ag sample positions

are $LOD_{Al} = 5.0 \cdot 10^{-6}$ and $LOD_{Ag} = 2.5 \cdot 10^{-6}$ in refractive index units (RIU), respectively. From these results we can conclude that the realized structure is an excellent candidate for biosensing applications, with resonance peaks at multiple spectral positions, which opens further possibilities in the domain of investigations of real-time protein adsorption.

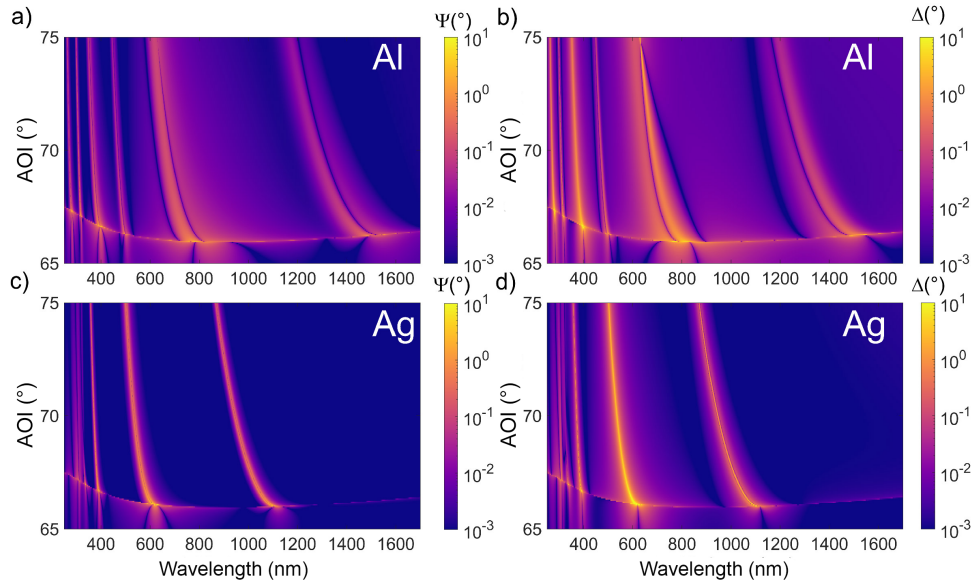


Figure 9: TMM-calculated differences in (Ψ, Δ) spectra for a $\Delta n_{water} = 10^{-4}$ change. Sub-figures a) and b) stand for Al, while sub-figures c) and d) for Ag.

Measurements at $x = 0$ and 1 were also carried out for demonstrating the sensitivity of the structure at $\theta = 73^\circ$ (Figs. 10c and 10d). Solutions of high-purity deionized (DI) water and isopropanol (VWR Chemicals) with various concentrations (2.5%, 5%, 7.5% and 10%) were introduced to the flow cell, with different refractive indices of $n_{isopropanol}^{2.5\% \dots 10\%} = 1.3324, 1.3339, 1.3356, 1.3376$ and 1.3390, respectively (obtained from refractometric measurements at $\lambda = 632$ nm and at room temperature). In the following, subscripts 1, 2, 3, and 4 are used to label the refractive indices of various concentrations of 2.5%, 5%, 7.5% and 10%, respectively. The difference spectra measured in the KR-cell are presented

1
2
3
4
5
6
7
8
9
10
11
12
13
14
15
16
17
18
19
20
21
22
23
24
25
26
27
28
29
30
31
32
33
34
35
36
37
38
39
40
41
42
43
44
45
46
47
48
49
50
51
52
53
54
55
56
57
58
59
60
61
62
63
64
65

in Figs. 10c and 10d for both ellipsometric angles. It is evident that Δ is more sensitive than Ψ , since the change is almost one-order of magnitude larger. For $n_{21} = 1.6 \times 10^{-3}$ RIU the biggest $\Delta\Delta_{21}^{Ag}$ difference for $x = 1$ is 70.05° positioned at $\lambda = 535.4$ nm, and $\Delta\Delta_{21}^{Al} = 36.38^\circ$ at $\lambda = 685.7$ nm. From these results the LOD_{Ag}^{meas} can be estimated to be $4.1 \cdot 10^{-6}$ RIU and $LOD_{Al}^{meas} = 7.9 \cdot 10^{-6}$ RIU.

The TMM-simulated results (Figs. 10a and 10b) show similar sensitivities. However, regarding the peak for $x = 1$ near $\lambda \approx 1000$ nm and for the UV-peaks for $x = 0$, higher sensing performance are predicted by the numerical calculations. This decrease in the performance can be attributed to various effects such as the emerging depolarization stemming from e.g., the angular spread of the incident light [55] or the inhomogeneity of layer thicknesses/compositions (e.g., latter being ≈ 1.5 % for Ag_xAl_{1-x} thin film) of the combinatorial layers under the light spot. Besides that the non-optimal performance of the deuterium lamp at these wavelengths also can have a significant effect on the sensitivities. Typical depolarization spectra from measurement are depicted in Fig. 6S.

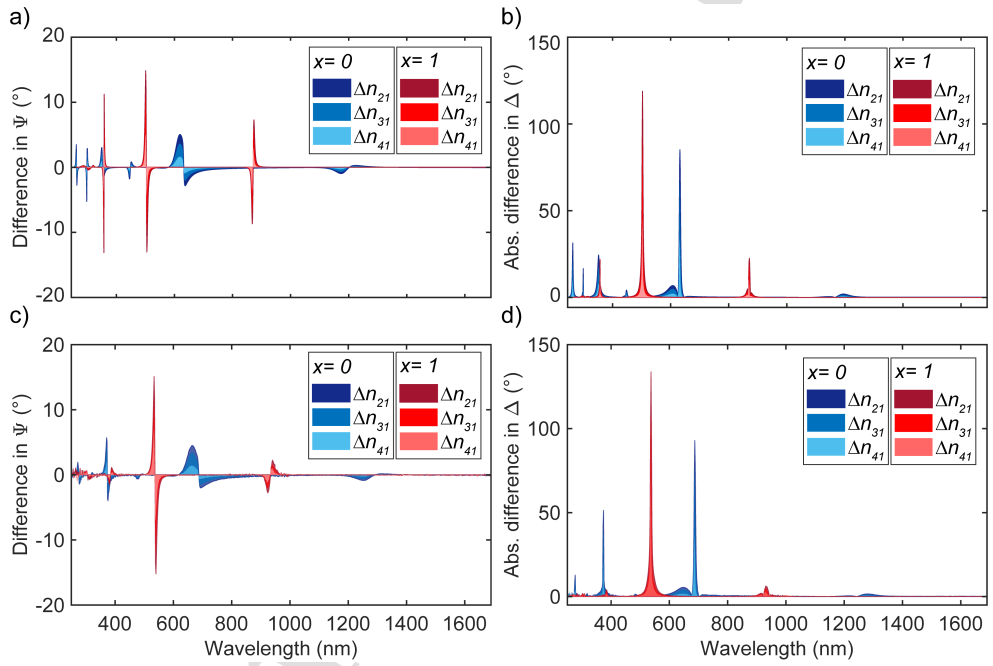


Figure 10: Difference of simulated [a) and b)] and measured [c) and d)] Ψ and Δ spectra at compositions $x = 0$ and 1 for various DI water-isopropanol solution ambient. Δn_{j1} denotes the refractive index difference at $\lambda = 632$ nm ($j = 2, 3, 4$).

Conclusions

In this study a combinatorial thin layer structure was introduced which is capable of the optical detection of minute changes in the refractive index of gas or liquid ambient. The combinatorial sample consists of an $\text{Ag}_x\text{Al}_{1-x}/\text{Si}_3\text{N}_4$ layer structure which was deposited on a FS glass slide by dual DC magnetron sputtering. It was shown that not only the composition can be covered in the whole range of ($0 \leq x \leq 1$), but also the thickness of the $\text{Ag}_x\text{Al}_{1-x}$ and Si_3N_4 layers can be tuned along a single sample. The optical properties of the combinatorial layer were characterized by KR SE from which the composition dependent trends in both ε_1 and ε_2 were obtained. These changes agree well with previously reported literatures; although this is the first study where ε is reported in the whole x range.

The sensing properties of the structure were also investigated numerically (at composition values of $x = 0$ and 1) for gas sensing applications and for biosensing applications in a liquid ambient. Based on the results it was verified that the realized structure is capable of highly sensitive detection in the UV-Vis-NIR wavelength ranges at a single AOI. Ellipsometric phase-sensitive measurements were also carried out from which detection limit values of $4.1 \cdot 10^{-6}$ RIU and $7.9 \cdot 10^{-6}$ RIU were measured at the Ag- and Al-sides of the chip. Our multi-spot, multi-angle tool with the compositionally graded surface realizes a "scanning resonant wavelength" capability, in which the spectral position of the highest sensitivity can be adjusted during the in-situ measurement.

Acknowledgements

Support from the National Development Agency Grants of OTKA Nr. K131515 and K129009 are greatly acknowledged. The work in frame of the 20FUN02 "POLight" project has received funding from the EMPIR programme co-financed by the Participating States and from the European Union's Horizon 2020 research and innovation programme.

1
2
3
4
5
6
7
8
9
10
11
12
13
14
15
16
17
18
19
20
21
22
23
24
25
26
27
28
29
30
31
32
33
34
35
36
37
38
39
40
41
42
43
44
45
46
47
48
49
50
51
52
53
54
55
56
57
58
59
60
61
62
63
64
65

445 **Competing interests**

The authors declare that they have no competing interests.

References

- [1] E. Wijaya, C. Lenaerts, S. Maricot, J. Hastanin, S. Habraken, J. Vilcot, R. Boukherroub, S. Szunerits, *Current Opinion in Solid State and Materials Science - CURR OPIN SOLID STATE MAT SCI* 15 (2011) 208–224. doi:10.1016/j.cossms.2011.05.001.
- [2] M. R. S. Dias, C. Gong, Z. A. Benson, M. S. Leite, *Advanced Optical Materials* 6 (2018) 1700830. URL: <https://onlinelibrary.wiley.com/doi/abs/10.1002/adom.201700830>. doi:<https://doi.org/10.1002/adom.201700830>. arXiv:<https://onlinelibrary.wiley.com/doi/pdf/10.1002/adom.201700830>.
- [3] C. Gong, M. S. Leite, *ACS Photonics* 3 (2016) 507–513. URL: <https://doi.org/10.1021/acsphotonics.5b00586>. doi:10.1021/acsphotonics.5b00586. arXiv:<https://doi.org/10.1021/acsphotonics.5b00586>.
- [4] J. P. McClure, J. Boltersdorf, D. R. Baker, T. G. Farinha, N. Dzuricky, C. E. P. Villegas, A. R. Rocha, M. S. Leite, *ACS Applied Materials & Interfaces* 11 (2019) 24919–24932. URL: <https://doi.org/10.1021/acsami.9b01389>. doi:10.1021/acsami.9b01389. arXiv:<https://doi.org/10.1021/acsami.9b01389>, PMID: 31044596.
- [5] C. Gong, A. Kaplan, Z. A. Benson, D. R. Baker, J. P. McClure, A. R. Rocha, M. S. Leite, *Advanced Optical Materials* 6 (2018) 1800218. URL: <https://onlinelibrary.wiley.com/doi/abs/10.1002/adom.201800218>. doi:<https://doi.org/10.1002/adom.201800218>. arXiv:<https://onlinelibrary.wiley.com/doi/pdf/10.1002/adom.201800218>.
- [6] M. Rebello Sousa Dias, M. S. Leite, *Accounts of Chemical Research* 52 (2019) 2881–2891. URL: <https://doi.org/10.1021/>

1
2
3
4
5
6
7
8
9 acs.accounts.9b00153. doi:10.1021/acs.accounts.9b00153.
10 arXiv:https://doi.org/10.1021/acs.accounts.9b00153, pMID:
11 31305980.
12
13

- 14 475 [7] P. West, S. Ishii, G. Naik, N. Emani, V. Shalaev, A. Boltas-
15 seva, *Laser & Photonics Reviews* 4 (2010) 795–808. URL:
16 https://onlinelibrary.wiley.com/doi/abs/10.1002/lpor.
17 200900055. doi:https://doi.org/10.1002/lpor.200900055.
18 arXiv:https://onlinelibrary.wiley.com/doi/pdf/10.1002/lpor.200900055.
19
20
21
22
23 480 [8] A. Bouhelier, T. Huser, H. Tamaru, H.-J. Güntherodt, D. W. Pohl,
24 F. I. Baida, D. Van Labeke, *Phys. Rev. B* 63 (2001) 155404.
25 URL: https://link.aps.org/doi/10.1103/PhysRevB.63.155404.
26 doi:10.1103/PhysRevB.63.155404.
27
28
29 [9] R. E. Peale, O. Lopatiuk, J. Cleary, S. Santos, J. Henderson, D. Clark,
30 L. Chernyak, T. A. Winningham, E. D. Barco, H. Heinrich, W. R.
31 485 Buchwald, *J. Opt. Soc. Am. B* 25 (2008) 1708–1713. URL: http:
32 //josab.osa.org/abstract.cfm?URI=josab-25-10-1708. doi:10.1364/
33 JOSAB.25.001708.
34
35
36
37
38 [10] L. Zhou, Y. Tan, J. Wang, W. Xu, Y. Yuan, W. Cai, S. Zhu, J. Zhu, *Nature*
39 490 *Photonics* 10 (2016). doi:10.1038/nphoton.2016.75.
40
41
42 [11] C. Haffner, D. Chelladurai, Y. Fedoryshyn, A. Josten, B. Baeuerle,
43 W. Heni, T. Watanabe, T. Cui, B. Cheng, S. Saha, D. Elder, L. Dal-
44 ton, A. Boltasseva, V. Shalaev, N. Kinsey, J. Leuthold, *Nature* 556 (2018).
45 doi:10.1038/s41586-018-0031-4.
46
47
48 495 [12] X. Deng, L. Li, M. Enomoto, Y. Kawano, *Scientific reports* 9 (2019) 3498.
49 doi:10.1038/s41598-019-39015-6.
50
51
52 [13] D. A. Bobb, G. Zhu, M. Mayy, A. V. Gavrilenko, P. Mead, V. I.
53 Gavrilenko, M. A. Noginov, *Applied Physics Letters* 95 (2009) 151102.
54
55
56
57
58
59
60
61
62
63
64
65

- 1
2
3
4
5
6
7
8
9 URL: <https://doi.org/10.1063/1.3237179>. doi:10.1063/1.3237179.
10
11 500 arXiv:<https://doi.org/10.1063/1.3237179>.
- 12
13 [14] G. Yang, X. Fu, J. Zhou, J. Opt. Soc. Am. B 30 (2013) 282–
14 287. URL: <http://josab.osa.org/abstract.cfm?URI=josab-30-2-282>.
15 doi:10.1364/JOSAB.30.000282.
16
17
- 18 [15] O. P. na Rodríguez, M. Caro, A. Rivera, J. Olivares, J. M. Perlado, A. Caro,
19 505 Opt. Mater. Express 4 (2014) 403–410. URL: <http://www.osapublishing.org/ome/abstract.cfm?URI=ome-4-2-403>. doi:10.1364/OME.4.000403.
20
21
22
- 23 [16] R. Collette, Y. Wu, A. Olafsson, J. P. Camden, P. D. Rack, ACS
24 Combinatorial Science 20 (2018) 633–642. URL: <https://doi.org/10.1021/acscombsci.8b00091>. doi:10.1021/acscombsci.8b00091.
25
26
27 510 arXiv:<https://doi.org/10.1021/acscombsci.8b00091>, PMID:
28 30277750.
29
30
31
- 32 [17] M. G. Blaber, M. D. Arnold, M. J. Ford, Journal of Physics: Condensed
33 Matter 22 (2010) 143201. URL: <https://doi.org/10.1088/0953-8984/22/14/143201>. doi:10.1088/0953-8984/22/14/143201.
34
35
36
- 37 [18] G. Subramania, A. J. Fischer, T. S. Luk, Applied Physics Letters
38 515 101 (2012) 241107. URL: <https://doi.org/10.1063/1.4770517>. doi:10.
39 1063/1.4770517. arXiv:<https://doi.org/10.1063/1.4770517>.
40
41
42
- 43 [19] R. Lazzari, J. Jupille, Surface Science 482-485 (2001) 823–828.
44 URL: [https://www.sciencedirect.com/science/article/pii/](https://www.sciencedirect.com/science/article/pii/S0039602801009359)
45 520 [S0039602801009359](https://www.sciencedirect.com/science/article/pii/S0039602801009359). doi:[https://doi.org/10.1016/S0039-6028\(01\)](https://doi.org/10.1016/S0039-6028(01)00935-9)
46 00935-9.
47
48
49
- 50 [20] D.-T. Nguyen, S. Vedraïne, L. Cattin, P. Torchio, M. Morsli,
51 F. Flory, J. C. Bernède, Journal of Applied Physics 112 (2012) 063505.
52 URL: <https://doi.org/10.1063/1.4751334>. doi:10.1063/1.4751334.
53
54
55 525 arXiv:<https://doi.org/10.1063/1.4751334>.
56
57
58
59
60
61
62
63
64
65

- 1
2
3
4
5
6
7
8
9 [21] R. S. Sennett, G. D. Scott, *J. Opt. Soc. Am.* 40 (1950) 203–211. URL: <http://www.osapublishing.org/abstract.cfm?URI=josa-40-4-203>. doi:10.1364/JOSA.40.000203.
- 10
11
12
13
14 [22] L. VJ, N. P. Kobayashi, M. S. Islam, W. Wu, P. Chaturvedi, N. X.
15 Fang, S. Y. Wang, R. S. Williams, *Nano Letters* 9 (2009) 178–182.
16 530 URL: <https://doi.org/10.1021/nl8027476>. doi:10.1021/nl8027476.
17 arXiv:<https://doi.org/10.1021/nl8027476>, PMID: 19105737.
- 18
19
20
21 [23] J. Zhang, D. M. Fryauf, M. Garrett, V. Logeeswaran, A. Sawabe, M. S.
22 Islam, N. P. Kobayashi, *Langmuir* 31 (2015) 7852–7859. URL: <https://doi.org/10.1021/acs.langmuir.5b01244>. doi:10.1021/acs.langmuir.
23 535 [5b01244](https://doi.org/10.1021/acs.langmuir.5b01244). arXiv:<https://doi.org/10.1021/acs.langmuir.5b01244>,
24 PMID: 26126182.
- 25
26
27
28
29 [24] M. Fahland, P. Karlsson, C. Charton, *Thin Solid Films* 392 (2001) 334–
30 337. URL: [https://www.sciencedirect.com/science/article/pii/](https://www.sciencedirect.com/science/article/pii/S0040609001010537)
31 [S0040609001010537](https://www.sciencedirect.com/science/article/pii/S0040609001010537). doi:[https://doi.org/10.1016/S0040-6090\(01\)](https://doi.org/10.1016/S0040-6090(01)01053-7)
32 540 [01053-7](https://doi.org/10.1016/S0040-6090(01)01053-7), 3rd International Conference on Coatings on Glass (ICCG).
- 33
34
35
36 [25] C. Zhang, D. Zhao, D. Gu, H. Kim, T. Ling, Y.-K. R. Wu,
37 L. J. Guo, *Advanced Materials* 26 (2014) 5696–5701. URL:
38 [https://onlinelibrary.wiley.com/doi/abs/10.1002/adma.](https://onlinelibrary.wiley.com/doi/abs/10.1002/adma.201306091)
39 [201306091](https://onlinelibrary.wiley.com/doi/abs/10.1002/adma.201306091). doi:<https://doi.org/10.1002/adma.201306091>.
40 545 arXiv:<https://onlinelibrary.wiley.com/doi/pdf/10.1002/adma.201306091>.
- 41
42
43
44 [26] Q. Hao, D. Du, C. Wang, W. Li, H. Huang, J. Li, T. Qiu, P. K. Chu,
45 *Scientific Reports* 4 (2014). doi:10.1038/srep06014.
- 46
47
48
49 [27] E. D. Palik, *Handbook of Optical Constants of Solids*, volume 1, San Diego:
50 Acad. Press, 1998.
51 550
- 52
53 [28] R. Adams, C. Nordin, K. Masterson, *Thin Solid Films* 72 (1980) 335–
54 339. URL: <https://www.sciencedirect.com/science/article/pii/>

0040609080900152. doi:[https://doi.org/10.1016/0040-6090\(80\)90015-2](https://doi.org/10.1016/0040-6090(80)90015-2).

- [29] S. Auer, W. Wan, X. Huang, A. G. Ramirez, H. Cao, *Applied Physics Letters* 99 (2011) 041116. URL: <https://doi.org/10.1063/1.3619840>. doi:10.1063/1.3619840. arXiv:<https://doi.org/10.1063/1.3619840>.
- [30] C. Zhang, N. Kinsey, L. Chen, C. Ji, M. Xu, M. Ferrera, X. Pan, V. M. Shalaev, A. Boltasseva, L. J. Guo, *Advanced Materials* 29 (2017) 1605177. URL: <https://onlinelibrary.wiley.com/doi/abs/10.1002/adma.201605177>. doi:<https://doi.org/10.1002/adma.201605177>. arXiv:<https://onlinelibrary.wiley.com/doi/pdf/10.1002/adma.201605177>.
- [31] H. Kim, T. Alford, *Journal of applied physics* 94 (2003) 5393–5395.
- [32] J. Yang, Guangand Sun, J. Zhou, *Journal of Applied Physics* 109 (2011) 123105. URL: <https://doi.org/10.1063/1.3592971>. doi:10.1063/1.3592971. arXiv:<https://doi.org/10.1063/1.3592971>.
- [33] G. Yang, X.-J. Fu, J.-B. Sun, J. Zhou, *Journal of Alloys and Compounds* 547 (2013) 23–28. URL: <https://www.sciencedirect.com/science/article/pii/S0925838812013928>. doi:<https://doi.org/10.1016/j.jallcom.2012.08.007>.
- [34] K. Diest, V. Liberman, D. Lennon, P. Welander, M. Rothschild, *Optics express* 21 (2013) 28638–50. doi:10.1364/OE.21.028638.
- [35] I. Tanabe, Y. Y. Tanaka, K. Watari, T. Hanulia, T. Goto, W. Inami, Y. Kawata, Y. Ozaki, *Scientific Reports* 7 (2017) 1.
- [36] G. Sáfrán, *Ultramicroscopy* 187 (2018) 50–55.
- [37] D. Sarid, *Phys. Rev. Lett.* 47 (1981) 1927–1930. doi:10.1103/PhysRevLett.47.1927.

- 1
2
3
4
5
6
7
8
9 [38] G. Nenninger, P. Tobiška, J. Homola, S. Yee, *Sensors and Actua-*
10 *tors B: Chemical* 74 (2001) 145–151. URL: <http://doi.org/10.1016/>
11 [s0925-4005%2800%2900724-3](http://doi.org/10.1016/s0925-4005%2800%2900724-3). doi:10.1016/s0925-4005(00)00724-3.
12 580
13
14 [39] C. Vernoux, Y. Chen, L. Markey, C. Spâchez, J. Arocas, T. Felder,
15 M. Neitz, L. Brusberg, J.-C. Weeber, S. Bozhevolnyi, A. Dereux, *Opti-*
16 *cal Materials Express* 8 (2018) 469 – 484. doi:10.1364/OME.8.000469.
17
18
19 [40] J.-Y. Jing, Q. Wang, W.-M. Zhao, B.-T. Wang, *Optics and Lasers in En-*
20 *gineering* 112 (2019) 103–118. doi:10.1016/j.optlaseng.2018.09.013.
21 585
22
23 [41] E. Kretschmann, H. Raether, *Zeitschrift für Naturforschung A* 23 (1968)
24 615–617. doi:10.1515/zna-1968-0424.
25
26 [42] T. Lohner, B. Kalas, P. Petrik, Z. Zolnai, M. Serényi, G. Sáfrán, *Applied*
27 *Sciences* 8 (2018) 826.
28
29
30 [43] B. Kalas, Z. Zolnai, G. Sáfrán, M. Serényi, E. Agocs, T. Lohner, A. Németh,
31 590 N. Q. Khánh, M. Fried, P. Petrik, *Scientific reports* 10 1 (2020) 19266.
32
33
34 [44] D. W. Lynch, W. Hunter, in: E. D. PALIK (Ed.), *Hand-*
35 *book of Optical Constants of Solids*, Academic Press, Boston,
36 1998, p. 341. URL: <http://www.sciencedirect.com/science/>
37 [article/pii/B9780080556307500183](http://www.sciencedirect.com/science/article/pii/B9780080556307500183). doi:[https://doi.org/10.1016/](https://doi.org/10.1016/B978-0-08-055630-7.50018-3)
38 [B978-0-08-055630-7.50018-3](https://doi.org/10.1016/B978-0-08-055630-7.50018-3).
39 595
40
41
42 [45] O. Blazquez, J. Lopez-Vidrier, S. Hernandez, J. Montserrat, B. Garrido,
43 *Energy Procedia* 44 (2014) 145–150. doi:10.1016/j.egypro.2013.12.021.
44
45
46 [46] B.-H. Liao, C.-N. Hsiao, *Appl. Opt.* 53 (2014) A377–A382. doi:10.1364/
47 *AO*.53.00A377.
48 600
49
50 [47] N. Mudgal, A. Saharia, K. Choure, A. Agarwal, G. Singh, *Applied Physics*
51 *A* 126 (2020). doi:10.1007/s00339-020-04126-9.
52
53
54 [48] B. Kalas, J. Nador, E. Agocs, A. Saftics, S. Kurunczi, M. Fried, P. Petrik,
55 *Applied Surface Science* (2017) S0169433217310802. URL: <http://doi.org/10.1016/j.apsusc.2017.05.001>.
56
57
58
59
60
61
62
63
64
65

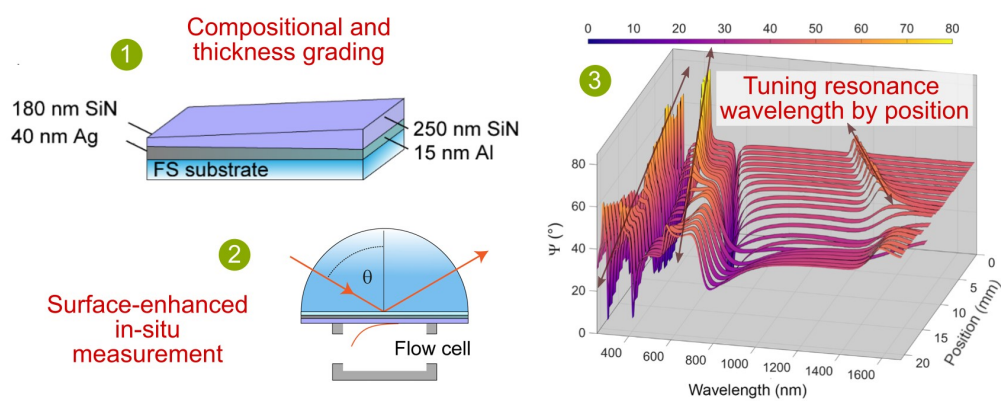
- 1
2
3
4
5
6
7
8
9
10
11
12
13
14
15
16
17
18
19
20
21
22
23
24
25
26
27
28
29
30
31
32
33
34
35
36
37
38
39
40
41
42
43
44
45
46
47
48
49
50
51
52
53
54
55
56
57
58
59
60
61
62
63
64
65
- 605 org/10.1016/j.apsusc.2017.04.064. doi:10.1016/j.apsusc.2017.04.
064.
- [49] A. S. Lambert, S. N. Valiulis, A. S. Malinick, I. Tanabe, Q. Cheng,
Analytical Chemistry 92 (2020) 8654–8659. URL: [https://doi.org/
10.1021/acs.analchem.0c01631](https://doi.org/10.1021/acs.analchem.0c01631). doi:10.1021/acs.analchem.0c01631.
610 arXiv:<https://doi.org/10.1021/acs.analchem.0c01631>, pMID:
32525300.
- [50] D. Gérard, S. K. Gray, Journal of Physics D: Applied Physics
48 (2014) 184001. URL: [https://doi.org/10.1088/0022-3727/48/18/
184001](https://doi.org/10.1088/0022-3727/48/18/184001). doi:10.1088/0022-3727/48/18/184001.
- 615 [51] K. Hinrichs, K.-J. Eichhorn, Ellipsometry of Functional Organic Surfaces
and Films, Springer Series in Surface Sciences 52, 2nd ed. ed., Springer
International Publishing, 2018.
- [52] R. M. A. Azzam, N. M. Bashara, Ellipsometry and Polarized Light, North-
Holland,, 1977.
- 620 [53] H. Arwin, M. Poksinski, K. Johansen, Applied optics 43 (2004) 3028–36.
doi:10.1364/AO.43.003028.
- [54] J. Nador, B. Kalas, A. Saftics, E. Agocs, P. Kozma, L. Korosi, I. Szekacs,
M. Fried, R. Horvath, P. Petrik, Opt Express 24 (2016) 4812–4823.
- [55] B. Kalas, K. Ferencz, A. Saftics, Z. Czigany, M. Fried, P. Petrik, Applied
625 Surface Science 536 (2021) 147869.
- [56] S. Cheon, K. Kihm, H. G. Kim, G. Lim, J. Park, J. Lee, Scientific Reports
4 (2014) 6364. doi:10.1038/srep06364.
- [57] A. D. Rakić, A. B. Djurišić, J. M. Elazar, M. L. Majewski, Appl. Opt. 37
(1998) 5271–5283. doi:10.1364/AO.37.005271.
- 630 [58] T.-W. Lee, S. Gray, Optics express 13 (2005) 9652–9. doi:10.1364/OPEX.
13.009652.

- 1
2
3
4
5
6
7
8
9 [59] T. E. Tiwald, D. W. Thompson, J. A. Woollam, W. Paulson, R. Hance,
10 Thin Solid Films 313-314 (1998) 661–666.
11
12 [60] C. C. Kim, J. W. Garland, H. Abad, P. M. Racciah, Phys. Rev. B 45 (1992)
13 11749–11767. URL: [https://link.aps.org/doi/10.1103/PhysRevB.45.](https://link.aps.org/doi/10.1103/PhysRevB.45.11749)
14 635 11749. doi:10.1103/PhysRevB.45.11749.
15
16 [61] D. De Sousa Meneses, G. Gruener, M. Malki, P. Echegut, Journal of Non-
17 Crystalline Solids 351 (2005) 0–129. URL: [http://doi.org/10.1016/j.](http://doi.org/10.1016/j.jnoncrysol.2004.09.028)
18 jnoncrysol.2004.09.028. doi:10.1016/j.jnoncrysol.2004.09.028.
19
20 [62] E. A. Irene, M. Losurdo, K. Hingerl, Ellipsometry at the Nanoscale, 1 ed.,
21 Springer-Verlag Berlin Heidelberg, 2013.
22
23 [63] J. Moré, Proceedings of the 1977 Dundee conference on numerical analysis
24 630 (1978) 630–668.
25
26 [64] K. S. B. D. Silva, V. J. Keast, A. Gentle, M. B. Cortie, Nanotechnology
27 28 (2017) 095202. URL: [https://doi.org/10.1088/1361-6528/aa5782.](https://doi.org/10.1088/1361-6528/aa5782)
28 645 28 (2017) 095202. URL: [https://doi.org/10.1088/1361-6528/aa5782.](https://doi.org/10.1088/1361-6528/aa5782)
29 doi:10.1088/1361-6528/aa5782.
30
31 [65] H. Ehrenreich, H. R. Philipp, Phys. Rev. 128 (1962) 1622–1629. doi:10.
32 1103/PhysRev.128.1622.
33
34 [66] G. Pribil, B. Johs, N. Ianno, Thin Solid Films s 455–456 (2004) 443–449.
35 650 doi:10.1016/j.tsf.2003.11.243.
36
37 [67] J. Gong, R. Dai, W. Zhongping, Z. Zhang, Scientific reports 5 (2015) 9279.
38 doi:10.1038/srep09279.
39
40 [68] R. Todorov, V. Katrova, P. Knotek, E. Cernoskova, M. Vlcek, Thin Solid
41 Films 628 (2017) 22. doi:10.1016/j.tsf.2017.03.009.
42
43 [69] V. P. Drachev, U. K. Chettiar, A. V. Kildishev, H.-K. Yuan, W. Cai, V. M.
44 Shalaev, Opt. Express 16 (2008) 1186–1195. URL: [http://opg.optica.](http://opg.optica.org/oe/abstract.cfm?URI=oe-16-2-1186)
45 org/oe/abstract.cfm?URI=oe-16-2-1186. doi:10.1364/OE.16.001186.
46
47
48
49
50
51
52
53
54
55
56
57
58
59
60
61
62
63
64
65

- 1
2
3
4
5
6
7
8
9 [70] V. S. a. Wenshan Cai, *Optical Metamaterials: Fundamentals and Applications*, 1 ed., Springer-Verlag New York, 2010.
10
11
12
13 [71] U. Kreibig, *Journal of Physics F: Metal Physics* 4 (2001) 999. doi:10.1088/
14 0305-4608/4/7/007.
15
16
17 [72] S. Van Gils, T. Dimogerontakis, G. Buytaert, E. Stijns, H. Terryn, P. Skel-
18 don, G. E. Thompson, M. R. Alexander, *Journal of Applied Physics*
19 98 (2005) 083505. URL: <https://doi.org/10.1063/1.2085315>. doi:10.
20 1063/1.2085315. arXiv:<https://doi.org/10.1063/1.2085315>.
21 665
22
23 [73] S. Xilian, R. Hong, H. Hou, Z. Fan, J. Shao, *Thin Solid Films* 515 (2007)
24 6962-6966. doi:10.1016/j.tsf.2007.02.017.
25
26
27 [74] Z. Ming, L. Yao-Peng, Z. Sheng, L. Ding-Quan, *Chinese Physics Letters* 32
28 (2015). doi:10.1088/0256-307X/32/7/077802.
29
30
31 [75] F. Mao, M. Taher, O. Kryshtal, A. Kruk, A. Czyska-Filemonowicz,
32 670 M. Ottosson, A. M. Andersson, U. Wiklund, U. Jansson, *ACS Ap-
33 plied Materials & Interfaces* 8 (2016) 30635-30643. URL: <https://doi.org/10.1021/acsami.6b10659>.
34 doi:10.1021/acsami.6b10659.
35 arXiv:<https://doi.org/10.1021/acsami.6b10659>, PMID: 27750408.
36
37
38 [76] M. D. Arnold, M. G. Blaber, *Opt. Express* 17 (2009) 3835-3847. doi:10.
39 1364/OE.17.003835.
40
41
42
43 [77] G. B. Irani, T. Huen, F. Wooten, *Phys. Rev. B* 3 (1971) 2385-2390.
44 URL: <https://link.aps.org/doi/10.1103/PhysRevB.3.2385>. doi:10.
45 1103/PhysRevB.3.2385.
46
47
48
49
50
51
52
53
54
55
56
57
58
59
60
61
62
63
64
65

pre-proof

Graphical Abstract (for review)

[Click here to access/download;Graphical Abstract \(for review\);TOC.pdf](#)

HIGHLIGHTS

- Combinatorial layer structure for phase-sensitive optical detection
- Combinatorial technique for changing both the composition and the layer thickness
- Limit of detection of 10^{-6} in refractive index units at each wavelength from ≈ 260 to ≈ 1500 nm
- Adjustable resonant peak positions by the angle and the spot location
- Demonstration in ellipsometric Kretschmann-Raether configuration

CRediT authorship contribution statement

B. Kalas: conceptualization, data curation, formal analysis, investigation, methodology, validation, writing of original draft and review editing; **G. Sáfrán:** methodology, investigation, conceptualization; **M. Serényi:** methodology, investigation, conceptualization; **M. Fried:** funding acquisition, project administration, resources; **P. Petrik:** conceptualization, methodology, funding acquisition, project administration, resources, investigation, validation, writing of original draft and review editing.

Declaration of interests

The authors declare that they have no known competing financial interests or personal relationships that could have appeared to influence the work reported in this paper.

The authors declare the following financial interests/personal relationships which may be considered as potential competing interests:

Journal Pre-proof